Supplement of Geosci. Model Dev., 15, 8181–8219, 2022
https://doi.org/10.5194/gmd-15-8181-2022-supplement

Geoscientific Model Development
Open Access

Supplement of

Importance of different parameterization changes for the updated dust cycle modeling in the Community Atmosphere Model (version 6.1)

Longlei Li et al.

Correspondence to: Longlei Li (ll859@cornell.edu)

Supplementary figures

Figure S1. Gravitational settling velocity ratio of ellipsoidal (V_{asp}) to spherical (V_{sph}) dust. Shape parameters for each major source (defined based on source apportionment) are taken from the global median of Huang et al., (2020) (see main text for information about this citation).

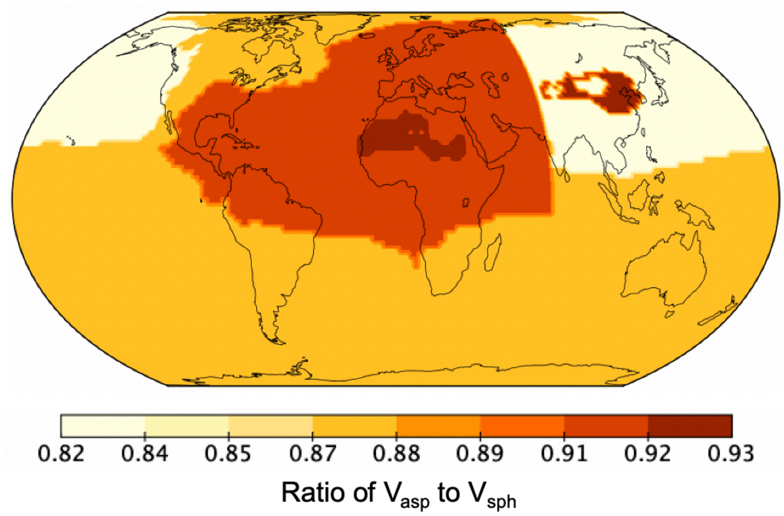

Figure S2. Influence of changing to PZ10 on the simulated dry deposition fluxes. Panel (a): fluxes from CAM6.α _MINE minus those from MINE_NEW_EMIS_SHAPE; Panel (b): fluxes from a test simulation with PZ10 included in CAM6.1 minus those from a test simulation with Z01 included in CAM6.1. Quantified change to the global annual mean of dry dust deposition equals to ~70 Tg by both methods. The number on top of each panel shows the global annual mean. See Table 2 for information about the case names.

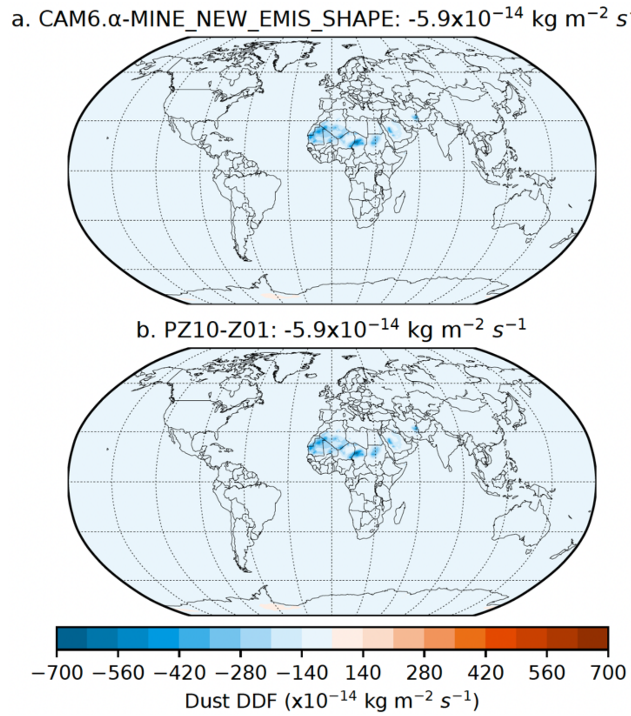

Figure S3. Comparison of the simulated dust loading (a), and deposition fluxes (b), and DOD (c) between the proposed new (CAM6.α) and default (CAM6.1) models on a grid-cell (a, b, and c) and regionally averaged basis (d). Numbers on top of panels (a-c) represent the global mean relative changes. The classic Taylor diagram compares CAM6.α against CAM6.1 as a reference (REF) in 21 sub-regions defined in Fig. S16. Both the standard deviation and temporal correlation (Kendall's τ coefficient) are obtained based on the modeled monthly dust loading/deposition fluxes/DOD in each of the sub-regions with seasonal cycle removed.

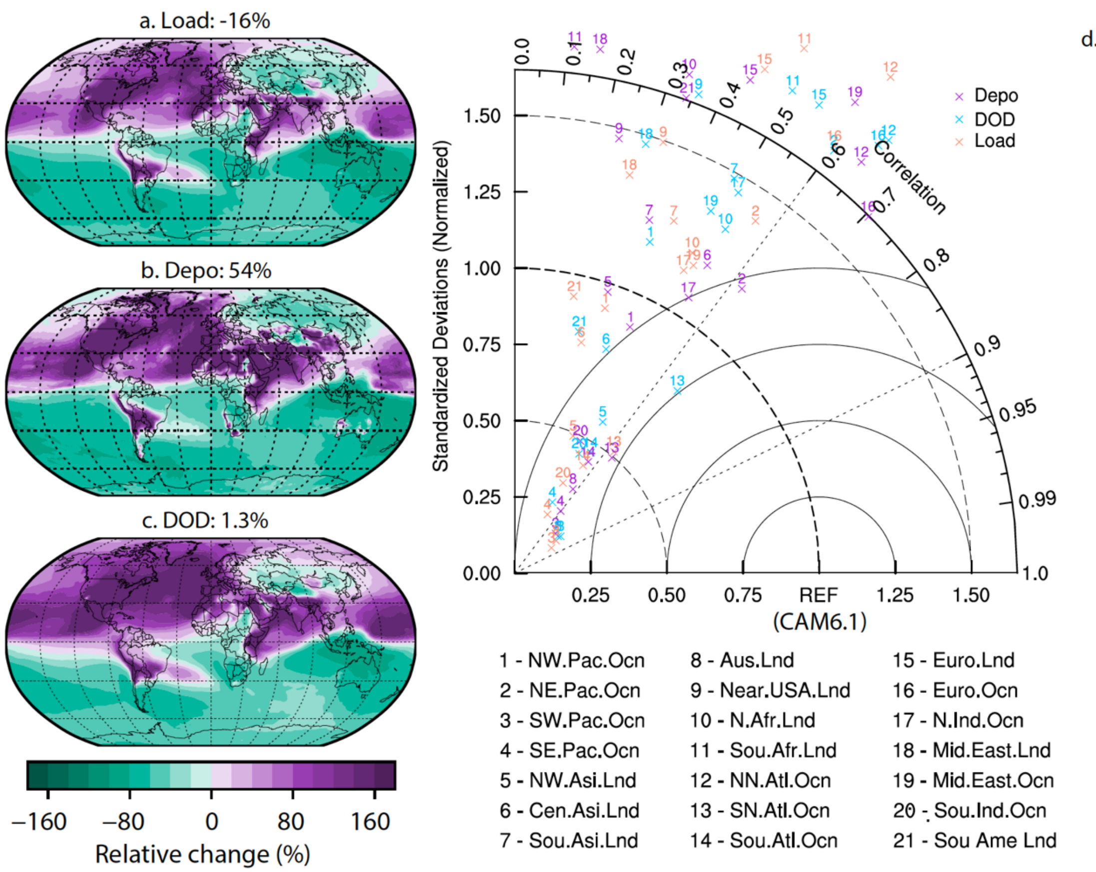

Figure S4. Comparison of modeled and observational surface concentration, deposition, and optical depth of dust (DOD). Dash lines represent 10:1 or 1:10 lines; inlet numbers denote Kendall's τ or root mean square error (RMSE). See Table 2 for information about the simulations indicated by the case names (e.g., MINE_BASE). See Table 2 for information about the case names.

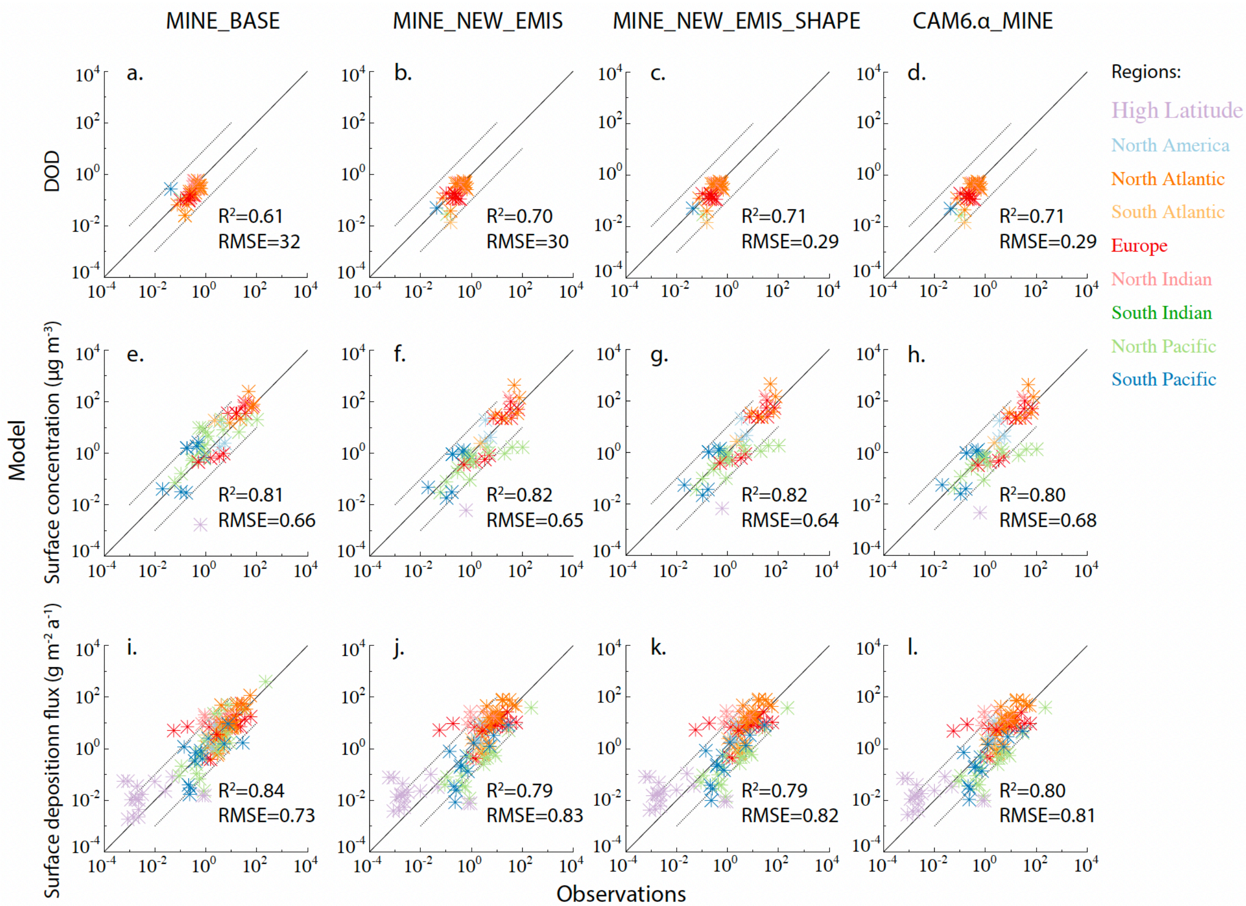

Figure S5. Dust wet deposition: percentage (a) (top color bar) and ratio of model results using BRIFT to those using DEAD (b; MINE_BASE and MINE_NEW_EMIS) (bottom color bar). The number on top of each panel shows the global annual mean.

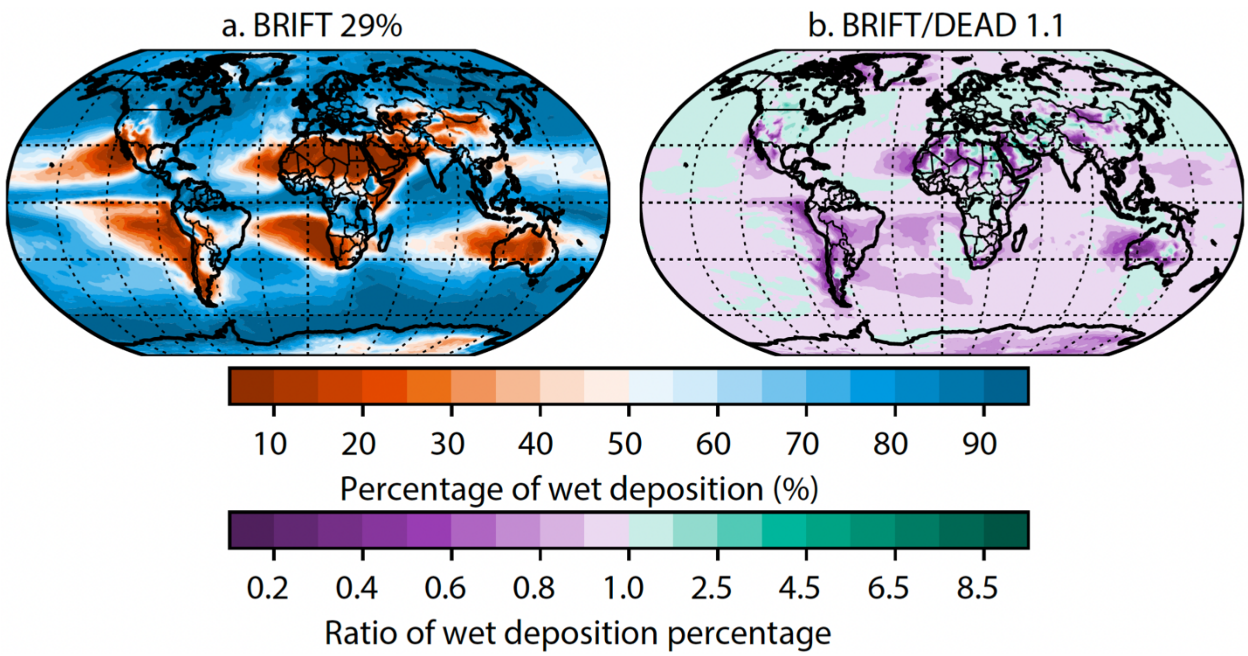

Figure S6. Seasonal cycle (x axis: 12 months) of DOD (unitless): a comparison of the simulated results (colored dots) to in situ (see site names in the figure titles) measurements (grey: Obs.). Colored shading columns indicate the observed peak month: blue shows where at least one of the five cases captured the peak, and purple shows where all cases failed to capture it. Colored numbers represent the Kendell's τ coefficient and RMSE between the model and observations. Superscript star "*" indicates a statistical significance of the model-observation correlation at the 95% confidence level. See Table 2 for information about the case names.

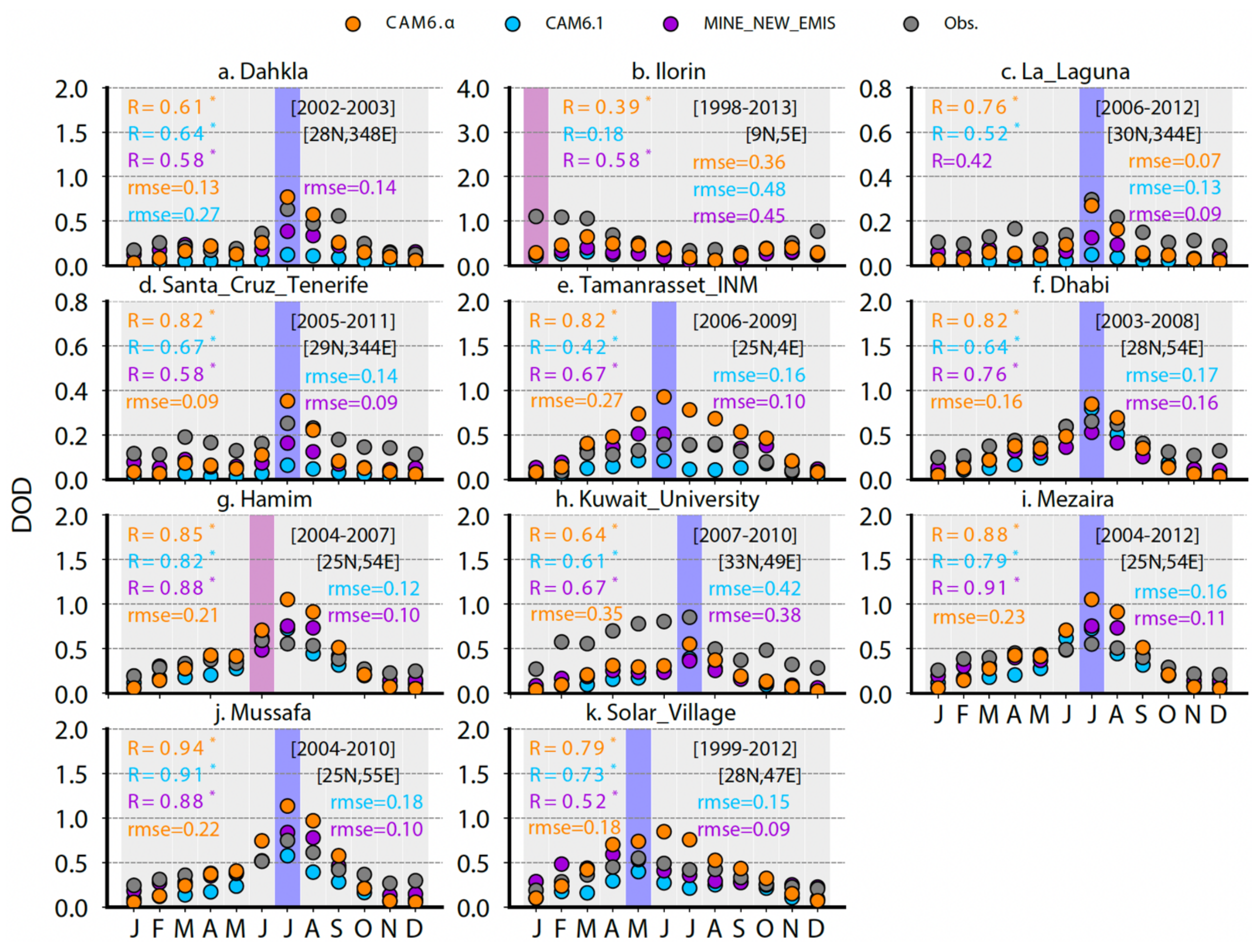

Figure S7. Comparison of seasonally (a: spring, MAM; b: summer, JJA; c, autumn, SON; d: winter, DJF) resolved regional DOD from models (y axis) to that (x axis) obtained in Ridley et al. (2016) with the region definition shown in their Fig. 1. Error bars represent the 2 standard deviations. Inlet numbers are RMSE and the spatial correlation (R; Kendall's τ coefficient). Note the size distribution with σ (GSD)=1.8 represents CAM5 size, and σ (GSD)=1.2 represents CAM6 size (see Table 1 in main text). All correlations are statistically significant at the confidence level of 95% except for CAM6.1 in DJF.

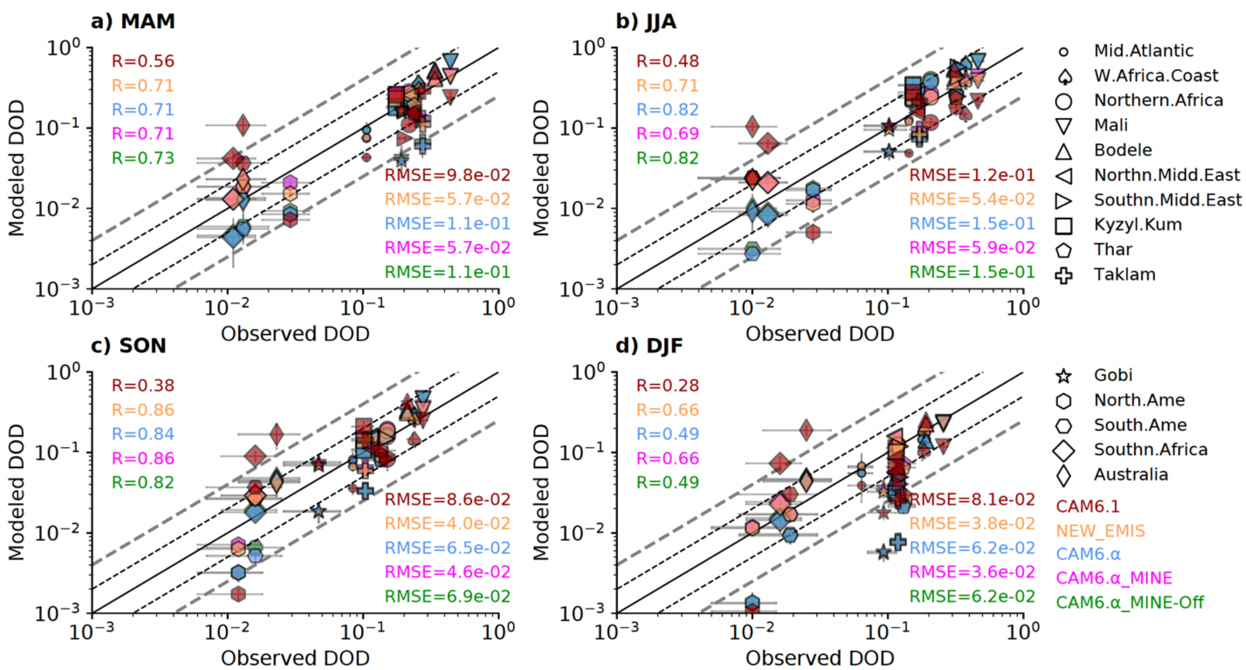

Figure S8. Similar to Fig. S6 but for surface dust concentrations (unit: μg cm^{-3}).

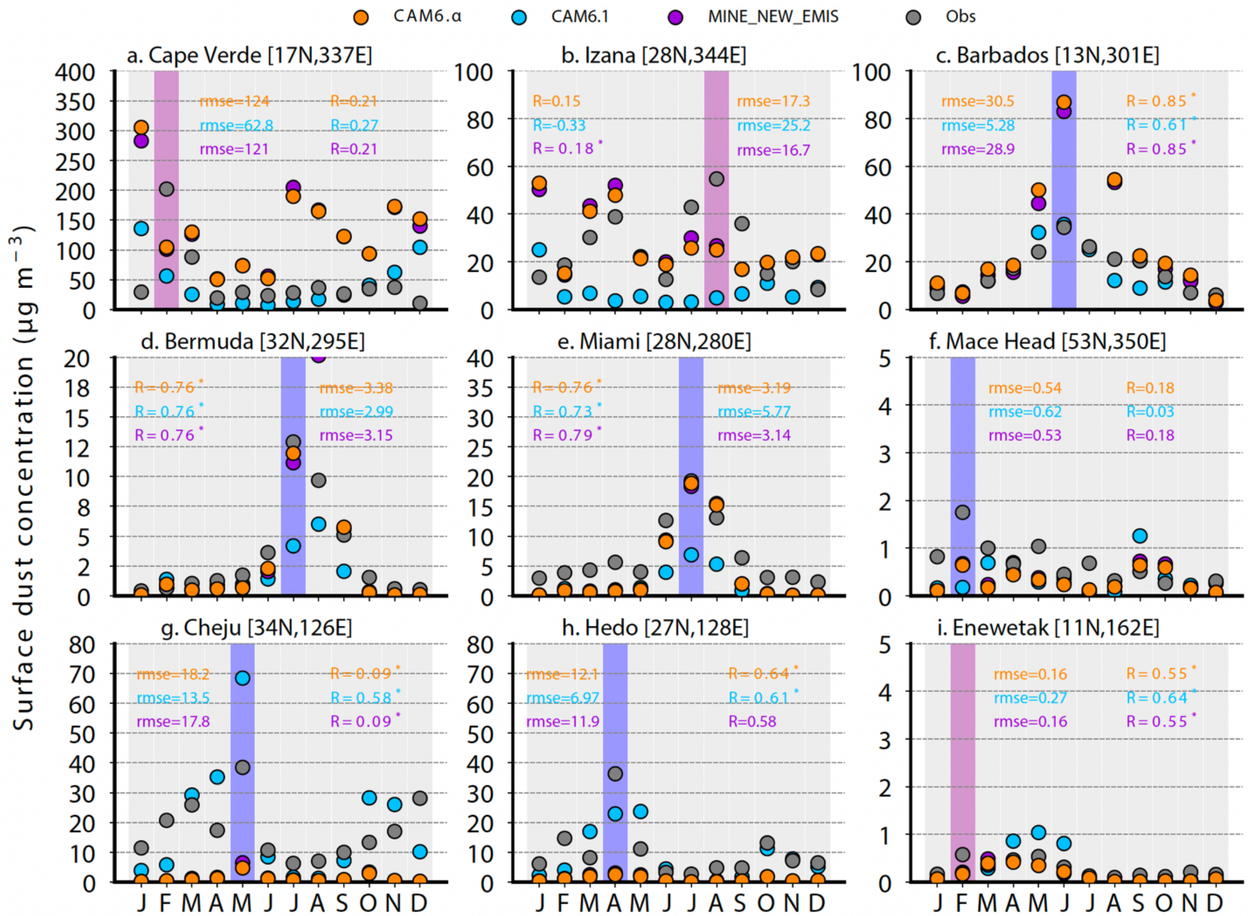

Figure S9. The same as Fig. S8 but for different sites as shown in the figure titles.

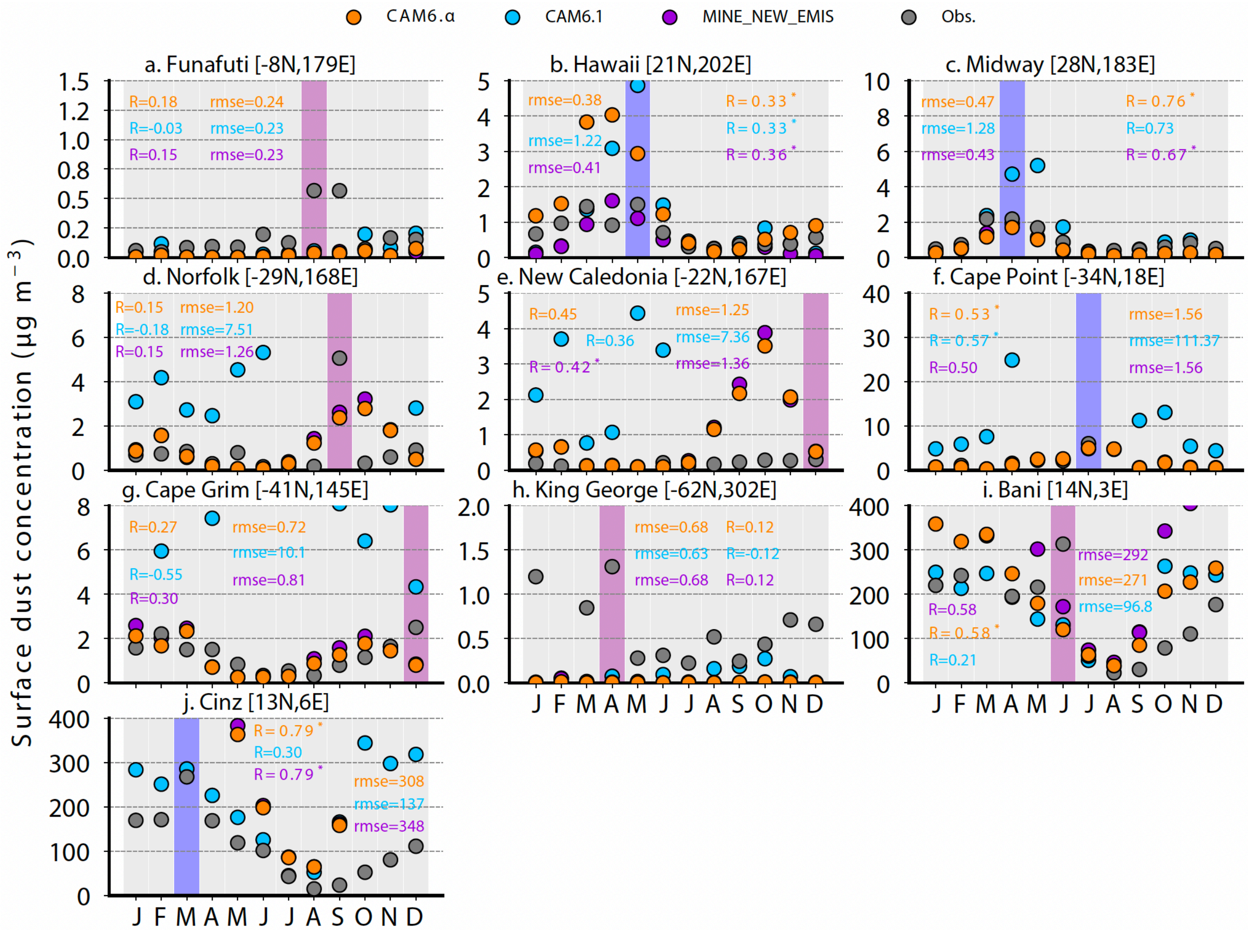

Figure S10. Normalized size distribution of dust between 0.2 and 10 μm for speciated-dust CAM6.α (red lines), CAM6.1 (blue lines), and observations (dot in orange colors) at Cabo Verde and Canary Island.

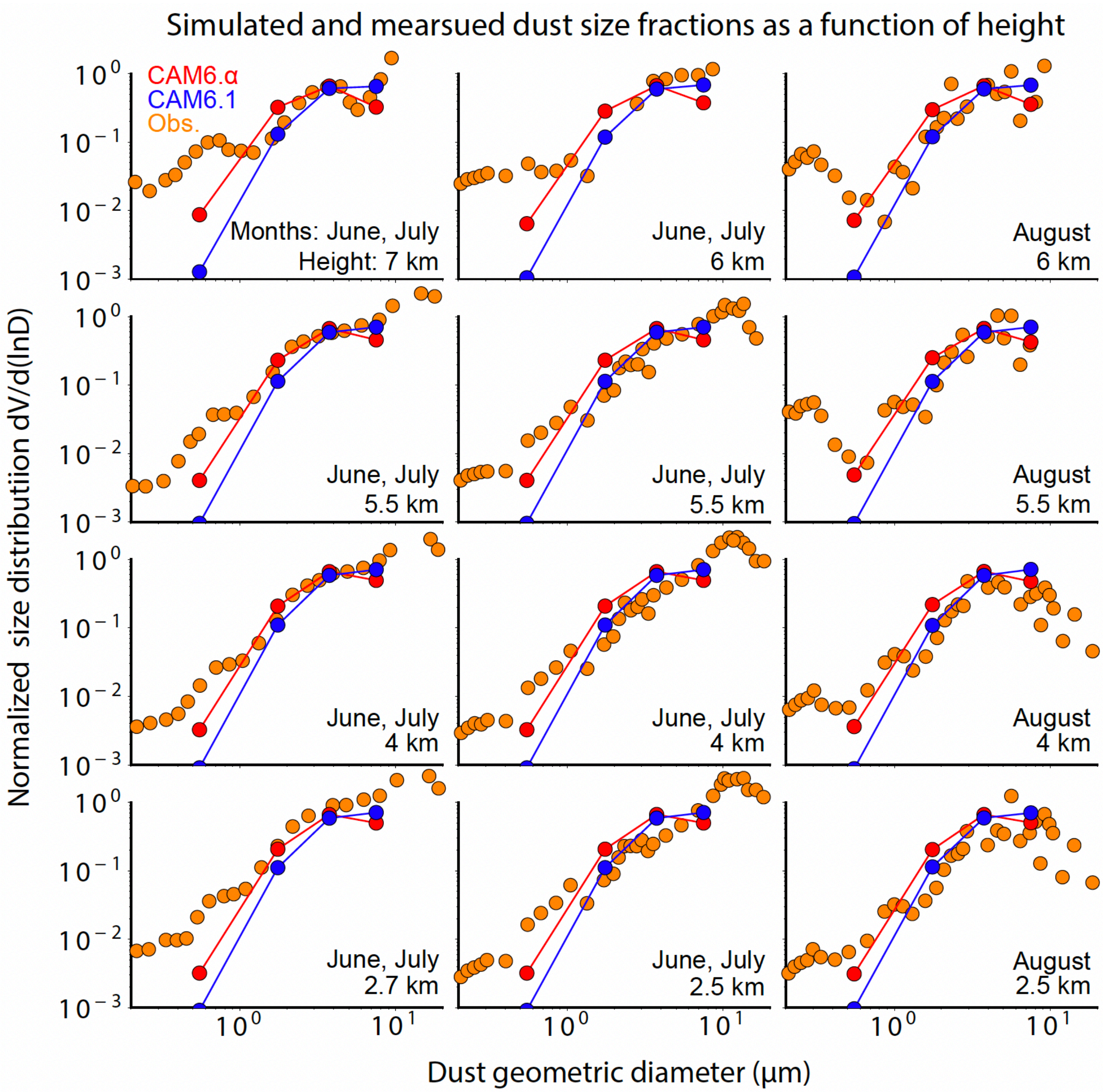

Figure S11. Dust emission flux rate (kg m^{-2} s^{-1}; rescaled up by 10^8) in the new model CAM6.α with the threshold gravimetric water content calculated following Fécan et al. (1999) (see the reference list in main text) using inversed clay fraction (b=1/f_{clay}). White color indicates zero emissions.

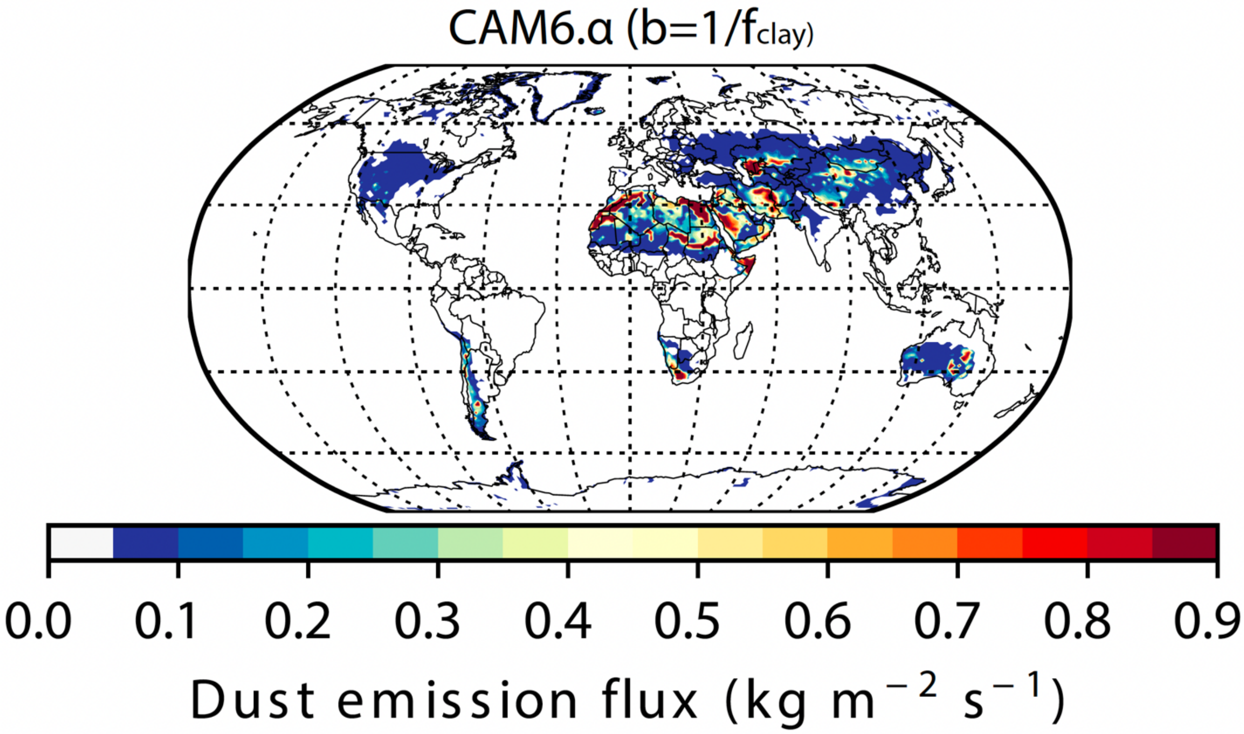

Figure S12. Change to the simulated (using offline dynamics and speciated-dust model) mass fraction of hematite, smectite, illite, feldspar, kalinite, and calcite aerosols by BRIFT (MINE_NEW_EMIS) relative to DEAD (MINE_BASE).

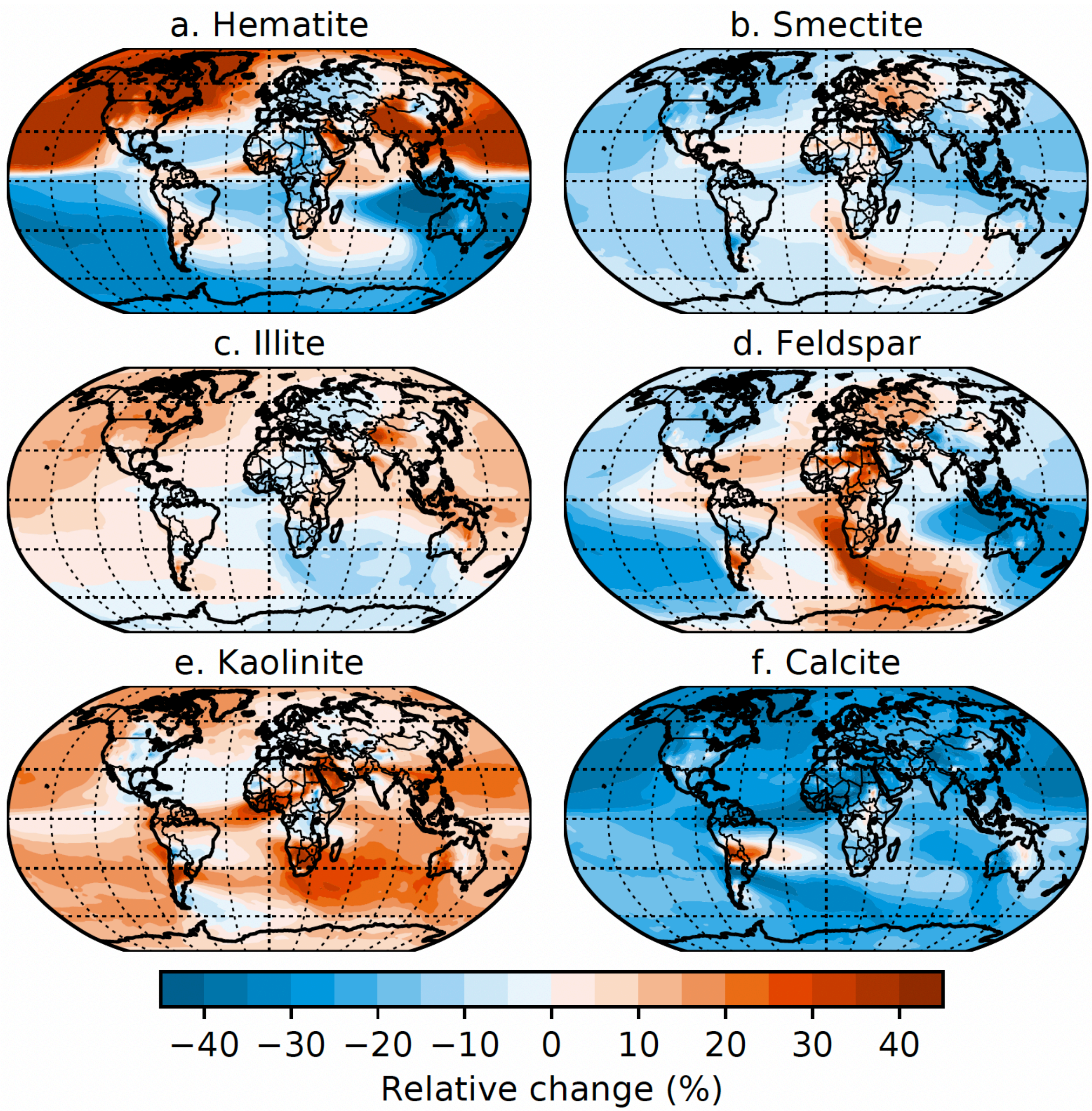

Figure S13. Impacts of the modifications on the modeling of surface dust dry deposition in the accumulation mode: ratio of model results using aspherical dust to those using spherical dust (a), PZ10 to Z01 (b), a combination of PZ10 and aspherical dust to that of Z01 and spherical dust (c), and BRIFT to DEAD (d). The number on top of each panel shows the global annual mean.

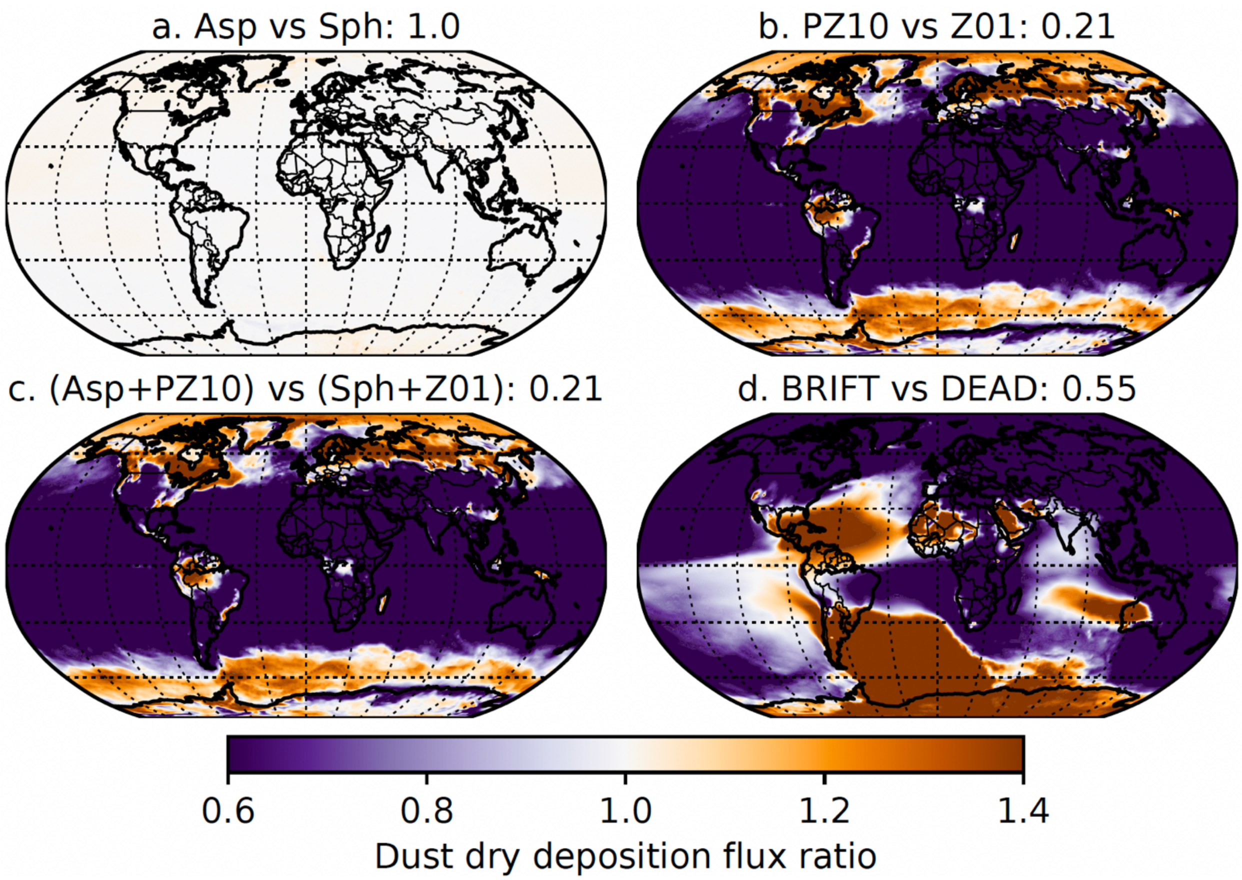

Figure S14. Impacts of the modifications on the modeling of dust total deposition: ratio of model results using aspherical dust to those using spherical dust (a), PZ10 to Z01 (b), a combination of PZ10 and aspherical dust to that of Z01 and spherical dust (c), and BRIFT to DEAD (d). The number on top of each panel shows the global annual mean.

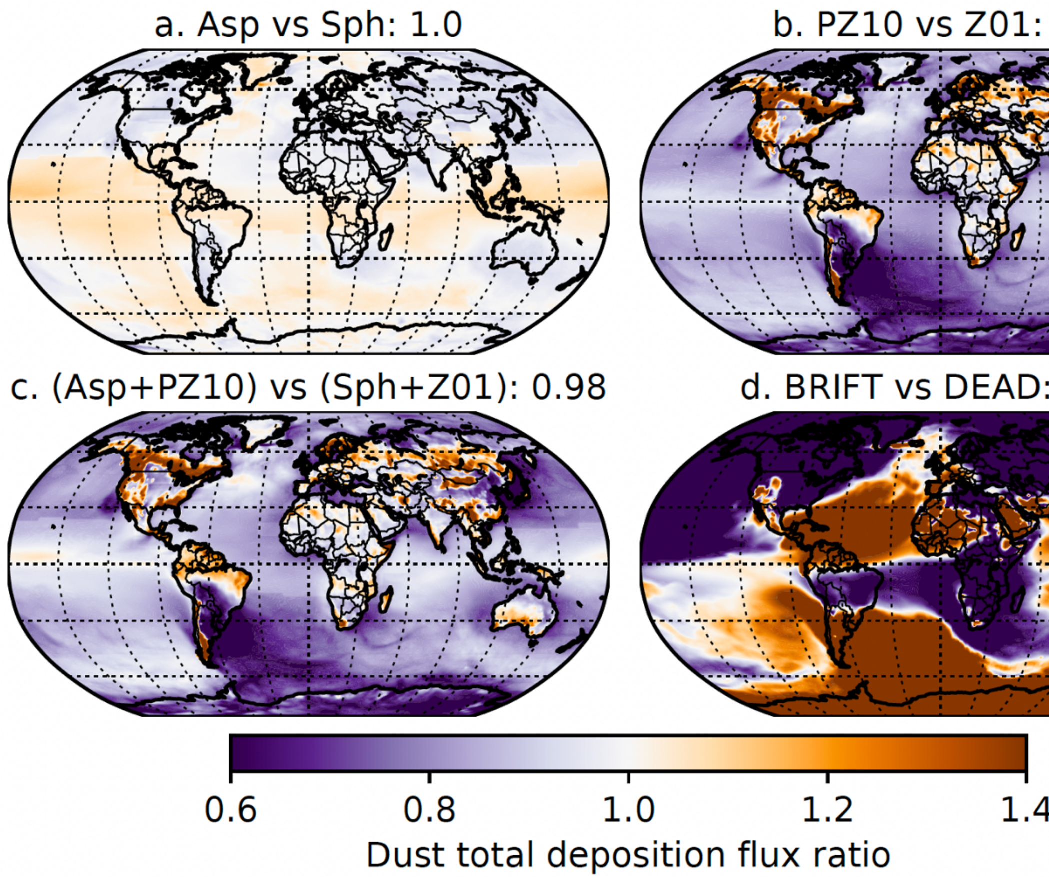

Figure S15. Same as Fig. S13 but for wet deposition.

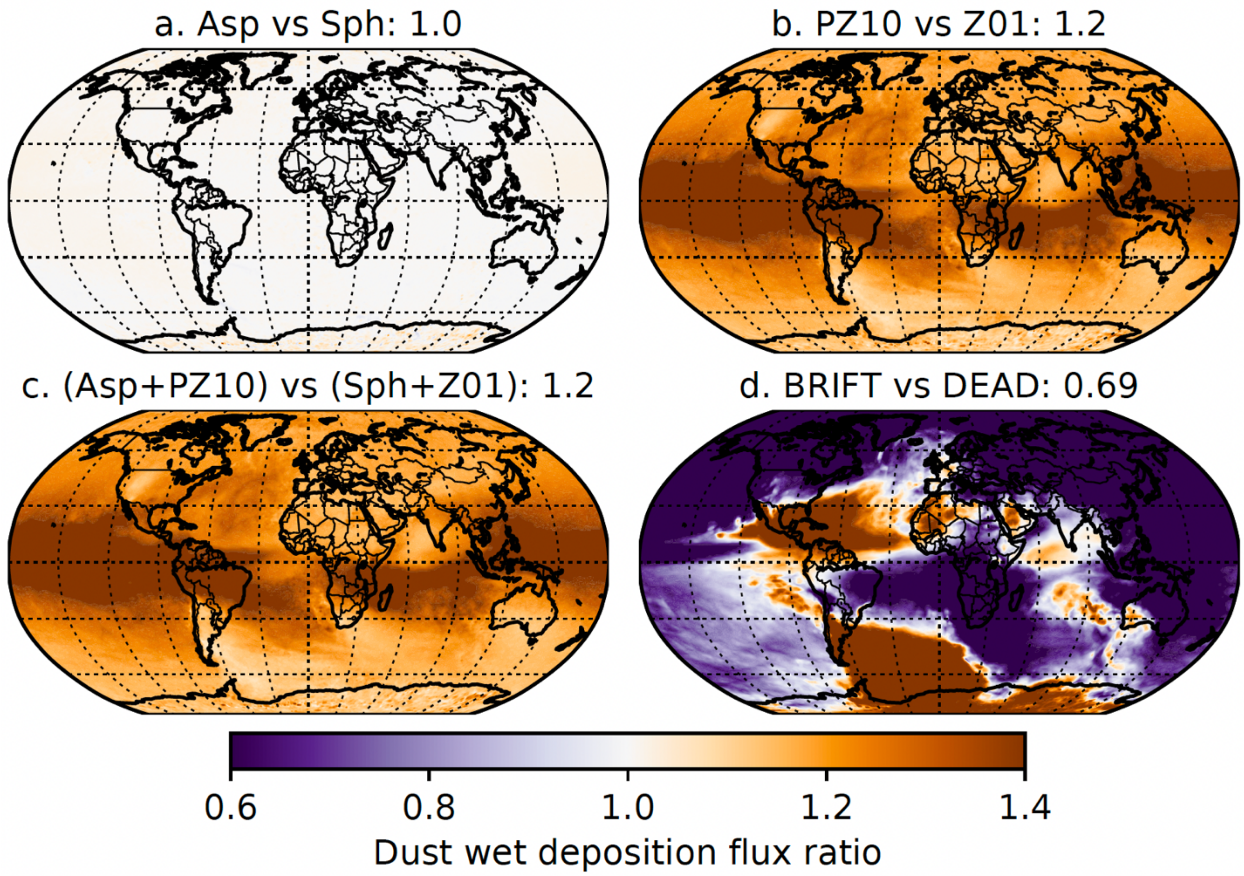

Figure S16. Sub-region division used in Fig. S3 and Fig. 7i: 1. NW Pac Ocn; 2. NE Pac Ocn; 3. SW Pac Ocn; 4. SE Pac Ocn; 5. NW Asian Lnd; 6. C Asian Lnd; 7. S Asian Lnd; 8. Australia Lnd; 9. USA Lnd; 10. N Afr Lnd; 11. S Afr Lnd; 12. NN Atl Ocn; 13. SN Atl Ocn; 14. S Atl. Ocn; 15. Euro Lnd; 16. Euro Ocn; 17. N Ind Ocn; 18. Mid East Lnd; 19. Mid East Ocn; 20. S Ind Ocn; 21. S Ame Lnd

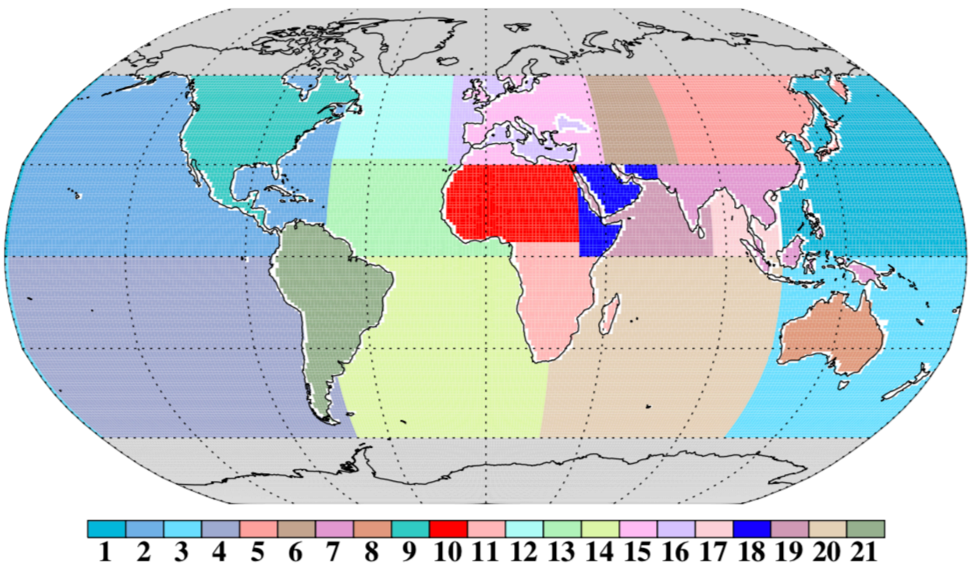

Figure S17. Dust net (shortwave plus longwave) DRE under all-sky conditions from CAM6.1 (a); its difference between CAM6.1 and CAM6.α (b); and difference between CAM6.α with the threshold gravimetric water content calculated following Fécan et al. (1999) (see the reference list in main text) using unity tuning factor and inversed clay fraction (CAM6.α_off) (c).

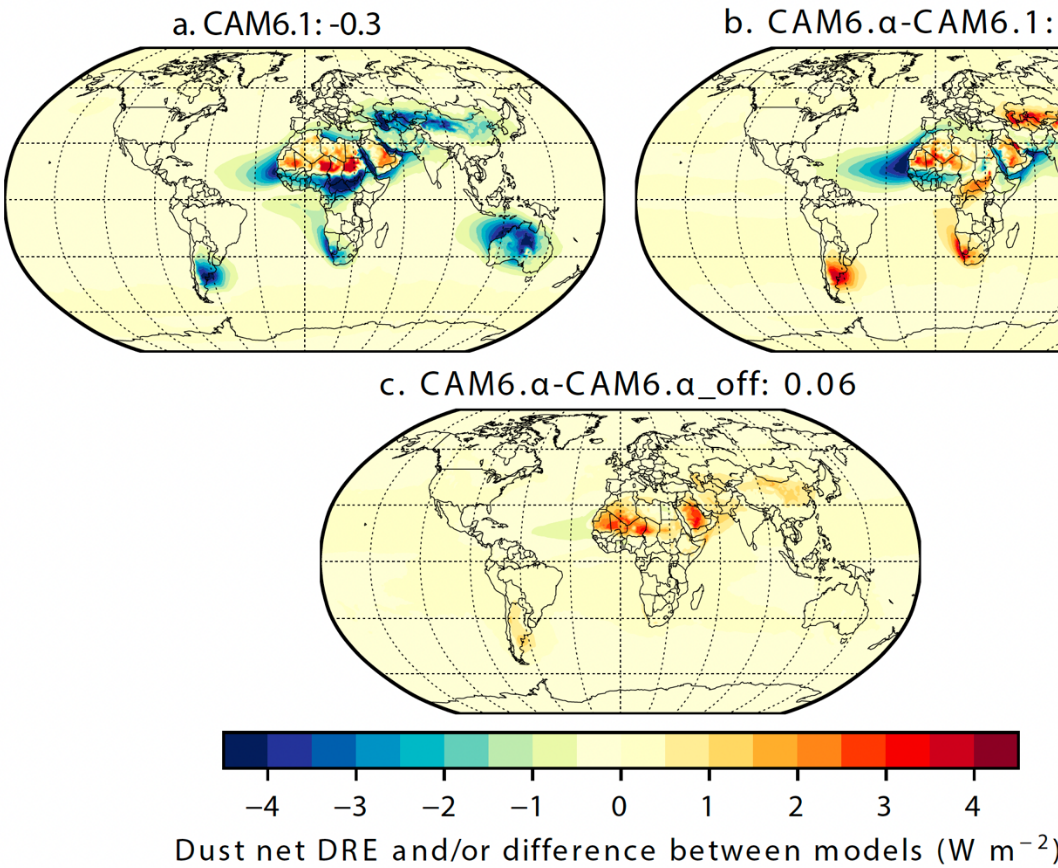

Figure S18. Comparison of the shortwave (SW) and longwave (LW) dust DRE under all-sky conditions with different coarse-mode size parameters (NEW_EMIS_SIZE, NEW_EMIS, and NEW_EMIS_SIZE_WIDTH; see Table 2 for information about the case names).

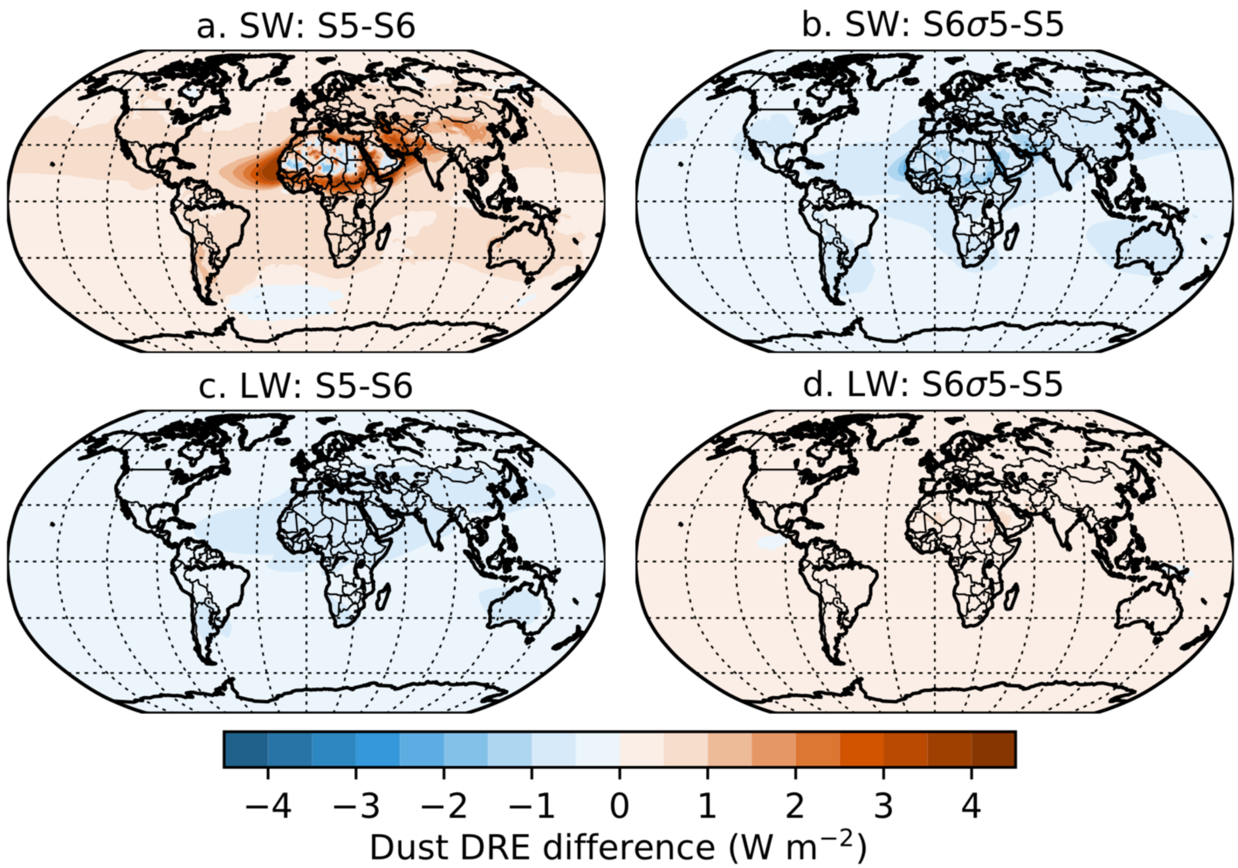

Supplementary tables

Table S1. Comparison of the three CESM test simulations for the year of 2006 with different values of the tuning parameter (b) to calculate the threshold gravimetric water content in the new dust emission scheme, against measurements. We used speciated-dust model with PZ10, BRIFT, the lifetime effect of dust asphericity, and offline dynamics. The measurements include AERONET dust optical depth (DOD) climatology, surface dust concentrations (unit: μg m^{-3}), and dust deposition fluxes (unit: g m^{-2} a^{-1}), as described in Section 3. RMSE: root mean square error.

Parameter b	Correlation coefficient (RMSE) on climatology		
	AERONET DOD	Surface dust concentrations (log space)	Dust deposition fluxes (log space)
0.5	0.74 (0.13)	0.83 (0.66)	0.72 (0.93)
1.0	0.68 (0.14)	0.82 (0.72)	0.77 (0.86)
2.0	0.66 (0.14)	0.83 (0.66)	0.79 (0.82)